s-Processing in Asymptotic Giant Branch Stars in the Light of Revised Neutron-Capture Cross Sections

Diego Vescovi * [ID] **and René Reifarth** [ID]

Institute for Applied Physics, Goethe University Frankfurt, Max-von-Laue-Strasse 1,
60438 Frankfurt am Main, Germany; reifarth@physik.uni-frankfurt.de
* Correspondence: vescovi@iap.uni-frankfurt.de

Abstract: Current AGB stellar models provide an adequate description of the s-process nucleosynthesis that occurs. Nonetheless, they still suffer from many uncertainties related to the modeling of the ^{13}C pocket formation and the adopted nuclear reaction rates. For many important s-process isotopes, a best set of neutron-capture cross sections was recently re-evaluated. Using stellar models prescribing that the ^{13}C pocket is a by-product of magnetic-buoyancy-induced mixing phenomena, s-process calculations were carried out with this database. Significant effects are found for a few s-only and branching point isotopes, pointing out the need for improved neutron-capture cross section measurements at low energy.

Keywords: nucleosynthesis; s-process; asymptotic giant branch stars; stellar abundances; nuclear reaction cross sections; chemically peculiar stars; circumstellar dust

1. Introduction

Asymptotic giant branch (AGB) stars are major production sources for heavy elements in the Universe. In particular, they were recognized to be responsible for the nucleosynthesis of the main and strong components (nuclei heavier than Sr) of the solar s-process (slow neutron-capture process) distribution (see, e.g., Busso et al. [1] for a review). AGB stars' interior consists of a carbon-oxygen core surrounded by a thin He-rich shell (He-intershell) and an extended H-rich envelope. These stars experience periodic He-shell flashes, called thermal pulses (TPs), inducing convective motions throughout the He-intershell that mix the products of the 3α reaction. The large amount of energy released during the TP also induces the expansion and cooling of the intershell region; as a consequence, the H-burning shell, previously active at the base of the envelope, dies down. After that, the convective envelope penetrates the He-intershell underlying region and brings freshly synthesized materials to the surface. This phenomenon is called third dredge-up (TDU). During a TDU, hydrogen is partially mixed from the convective envelope into the ^{12}C-rich He-intershell, where it is consumed through the ^{12}C(p, γ)^{13}N(β^{+})^{13}C chain, thus forming a ^{13}C-enriched layer, the so-called ^{13}C pocket. Such a ^{13}C burns in radiative conditions, when the temperature attains $\sim$90 MK, via the ^{13}C(α, n)^{16}O reaction during the long interpulse phase separating two subsequent TPs [2]. The ^{13}C(α, n)^{16}O reaction is the main source through which low-mass AGB stars release neutrons and produce s-elements (see, e.g., Cristallo et al. [3]). An additional neutron burst is driven by the ^{22}Ne(α, n)^{25}Mg reaction that is only marginally triggered at the base of the convective TP, due to the moderate temperatures ($T \lesssim 300$ MK).

To date, the mechanism responsible for the creation of the ^{13}C pocket is far from being well known. Several mixing processes have been proposed over the last years, involving convective overshoot [4], rotation-induced mixing [5–7], opacity-induced overshoot [8–10], or mixing induced by internal gravity waves [11–13]. More recently, the suggestion that stellar magnetic activity might be responsible for the formation of the ^{13}C pocket through

mixing induced by magnetic buoyancy has been proposed [14,15]. Post-process calculations of such a ^{13}C reservoir have shown to be able to reproduce the distribution of s-elements in the solar main component [15], heavy-element isotopic compositions of presolar grains [16], and most of n-capture elements abundances observed in Ba-stars and post-AGB stars [17]. These studies have been confirmed by numerical simulations of the formation of a magnetically-buoyancy-induced ^{13}C pocket in a new series of FRUITY stellar evolutionary models [18]. New FRUITY Magnetic models have also been found to be successful in reproducing the observed fluorine vs. average s-element enhancements in intrinsic carbon and extrinsic stars [19], and in a Galactic chemical evolution context, the observed trends of yttrium abundance in the inner part of the Galactic disk [20].

Besides the complexities associated with the modeling of the ^{13}C pocket formation, AGB s-process predictions also show large sensitivity to the adopted (n, γ) reaction rates. To date, the vast majority of experimentally measured neutron-capture cross sections are known with a precision of a few percent (see, e.g., Käppeler et al. [21]). For detailed AGB s-process nucleosynthesis simulations, Maxwellian averaged cross sections (MACS) ranging from thermal energies of about 8 keV, proper of the ^{13}C pocket radiative burning, to about 23–25 keV, during a TP, have to be considered. To cover the whole energy range, energy-differential cross sections are needed in the neutron energy region between about 0.1 keV and 1 MeV [21,22]. When experimental data in this range is missing, evaluated cross sections from data libraries have to be taken into account. In addition, many of the available experimental measurements, based on activation and time-of-flight (TOF) techniques, were performed relative to gold cross section as a standard. Recently, TOF measurements of the energy-dependent gold cross section [23,24] found a $\sim$5% higher value than the recommended cross section used as a standard for astrophysical applications [25]. The adoption of the new recommended value for the ^{197}Au(n, γ)^{198}Au have been studied for several TOF measurements in Reifarth et al. [22], in which several measurements carried out relative to this standard were re-examined. For these, a corresponding set of new recommended MACS was also provided. The stellar neutron cross section database "ASTrophysical Rate and rAw data Library" (ASTRAL) presents a list of these re-evaluated experimental MACS for energies between $kT = 1$ keV and 500 keV. The current version "v0" includes 64 new recommended cross sections (see Reifarth et al. [22] for more details).

In this work, the recommended MACS from the ASTRAL v0 database are used to investigate the impact on the s-process nucleosynthesis occurring in low-mass AGB stars, by computing selected stellar models. The results are then compared with those obtained by the previously adopted set of (n, γ) cross sections and with isotopic ratios of heavy elements measured in presolar SiC grains.

2. Stellar Models

Stellar models presented in this work have been computed with the FUNS (FUll Network Stellar) evolutionary code; see Straniero et al. [26] and references therein). The adopted network includes almost 500 isotopes (from H to Bi) and more than 800 nuclear reactions. Low-temperature C-enhanced molecular opacities computed by means of the ÆSOPUS tool [27] are used to take into account the variation of the envelope chemical composition determined by the carbon dredge-up during the TP-AGB phase [28]. A scaled-solar composition as provided by Lodders [29] is adopted. Accordingly, a mixing-length parameter $\alpha_{\mathrm{m.l.}}$ = 1.86, has been derived by computing a standard solar model (see Vescovi et al. [30] for more details on the followed procedure). For the mass-loss rate, we adopted a Reimers' formula with $\eta = 0.4$ for the pre-AGB evolution, while for the AGB phase, we used the rate as derived by Abia et al. [31]. In Vescovi et al. [18], mixing triggered by magnetic buoyancy was implemented in the FUNS code starting from the formalism developed by Nucci and Busso [32]. In brief, during a TDU, the peculiar density profile of the radiative layers below the convective envelope guarantees that if magnetic flux tubes are there formed, they are subject to buoyancy phenomena and can induce a stable mass circulation. In particular, the formation and buoyant rise of magnetic flux tubes in the He-

intershell of an AGB star may induce, for mass conservation, the partial mixing of hydrogen necessary for the development of the ^{13}C pocket. The efficiency of such mixing relies on the magnitude of the toroidal field necessary for the occurrence of magnetic buoyant instabilities and the initial velocity of magnetic flux tubes. Vescovi et al. [18] found that close-to-solar metallicity AGB models computed with a single configuration for the toroidal field strength ($B_\varphi = 5 \times 10^4$ G) and the initial buoyant velocity ($u_{\rm p} = 5 \times 10^{-5}$ cm s^{-1}), are able to account for the majority of the heavy-element isotope ratios measured in presolar silicon carbide (SiC) grains (see Vescovi et al. [18] for more details). In all the models presented in this work, we adopted the same configuration choice.

In order to assess the impact of the new (n, γ) cross sections evaluation on the s-process, we computed three models of an AGB star with mass $M = 2\,M_\odot$ and metallicity $Z = 0.01, 0.0167\,(\equiv Z_\odot), 0.02$, adopting two different sets of n-capture cross sections. In the reference models (hereinafter REF) we adopted the same nuclear network used in Vescovi et al. [18], while in the new models (hereinafter NEW) we adopted for 64 different cross sections the recent re-evaluation proposed by Reifarth et al. [22] (ASTRAL v0 database), where a detailed list of isotopes can be found.

3. Results and Discussion

In Figure 1, we report the heavy-isotope surface composition of a star with $M = 2\,M_\odot$ and metallicity $Z = 0.02$ for REF and NEW cases.
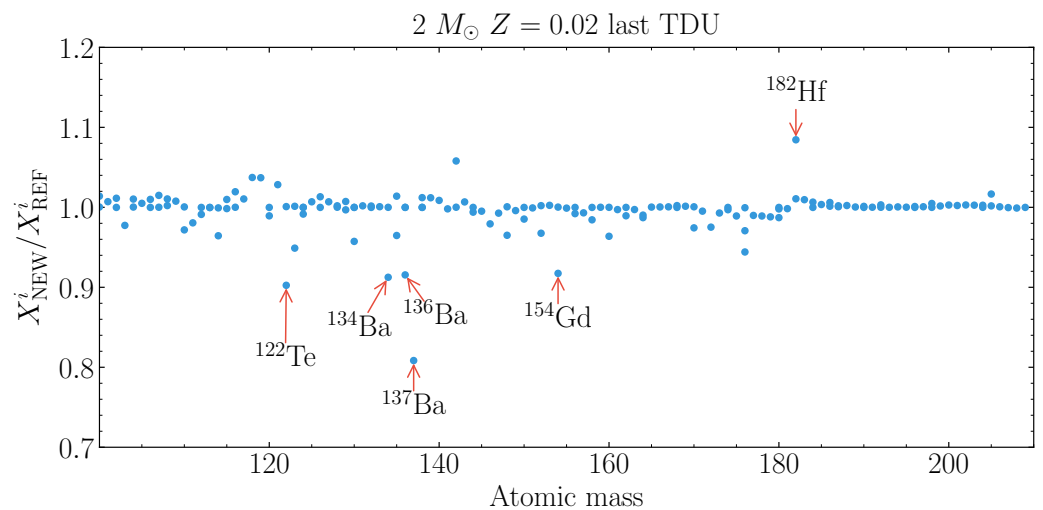
Figure 1. Ratio between the final heavy-isotopes surface distributions of the NEW case with respect to the REF case (see text for details) for an AGB model with initial mass $M = 2\,M_\odot$ and metallicity $Z = 0.02$. Enlightened are isotopes whose variation is $\gtrsim$10%.

The NEW model shows small variations ($\lesssim$5%) for the vast majority of the isotopes. Differences larger than $\sim$10% are obtained for ^{122}Te, ^{134}Ba, ^{136}Ba, and ^{154}Gd, whose production has been decreased mostly due to an increased MACS of the corresponding (n, γ) cross section (see Table 1). All of these isotopes are of pure s-process origin (s-only), being shielded against the β-decay chains from the r-process by stable isobars. The production of the s-dominated ^{137}Ba isotope is found to decrease by $\sim$20%, while the production of the short-lived isotope ^{182}Hf is enhanced by about 10%.

Table 1. Maxwellian averaged capture cross section (in mb) from ASTRAL v0 data set for kT = 30 keV. The values are compared with those of the REF data set.

Isotope	ASTRAL v0	Source	REF	Source
^{122}Te	332	[22]	295	[33]
^{134}Ba	186	[22]	176	[33]
^{136}Ba	67	[22]	61	[33]
^{137}Ba	90	[22]	76	[33]
^{142}Nd	36	[22]	35	[33]
^{154}Gd	1088	[22]	880	[34]
^{175}Lu	1299	[22]	1146	[33]
^{176}Lu	1744	[22]	1639	[35]
^{176}Hf	664	[22]	626	[36]

The abundance of ^{122}Te is potentially affected by the β-decay of the branch point isotope ^{122}Sb. However, at TP temperatures, its half-life is of the order of a few hours, [37] so that the decay channel largely dominates over the neutron-capture rate. The abundance variation of ^{122}Te is therefore ascribed to the enhanced MACS (+13% at 30 keV; see Table 1). The production of the two s-only isotopes ^{134}Ba and ^{136}Ba occurs both during the ^{13}C pocket and the TP phases. Despite the fact the both these isotopes are underproduced in the NEW model with respect to the REF model, the ^{134}Ba/^{136}Ba ratio is however not modified, since it is largely sensitive to the branch at ^{134}Cs, in particular to its β^--decay rate which decreases up to two orders of magnitude at 300 MK [37]. The ^{137}Ba/^{136}Ba ratio instead decreases by $\sim$12%. The final abundance of ^{154}Gd is determined by the competition between neutron capture on ^{154}Gd and β-decay rate of the close unstable isotope ^{154}Eu (see also Mazzone et al. [34]); as a whole, the decrease of the ^{154}Gd is slightly lower than the change of the neutron-capture cross sections (+24% at 30 keV). The production of the short-lived ^{182}Hf ($t_{1/2}$ = 8.9 Myr) is regulated by the branch at ^{181}Hf. According to Takahashi and Yokoi [37], its half-life strongly reduces during TPs, passing from a terrestrial value of 42.39 d to 1.26 d at 300 MK. This causes the s-path to proceed towards ^{182}W and the ^{182}Hf production to be low. However, the radiogenic contribution of ^{182}Hf occurring at the end of the TP-AGB phase is important to explain the solar abundance of ^{182}W. Present AGB estimations for the s-process main component can account for 65–70% of solar ^{182}W [17,38], while its r-process contribution is well justified by the Galactic enrichment of r-process elements [39]. However, Lugaro et al. [40] have pointed out that the present AGB contributions to ^{182}Hf and ^{182}W may have so far been underestimated. Based on the work of Bondarenko et al. [41], Lugaro et al. [40] suggested that the β-decay rate in stellar conditions remains pretty unchanged with respect to its terrestrial value, thus allowing an increased feeding of ^{182}Hf and, in turn, of ^{182}W after the TP-AGB phase. In this sense, further experimental evidence is demanding. In our computations, we cautiously adopt the decay rate given by Takahashi and Yokoi [37] for ^{181}Hf. By using the new ASTRAL v0 values for (n, γ) cross section in our calculations, the ^{182}Hf is increased by $\sim$10%. This is due to the enhanced MACS for hafnium isotopes, whose net effect is to increment the neutron density and thus the neutron-capture strength of the branching point at the unstable ^{181}Hf. This result is of relevance for the origin of ^{182}Hf in the early Solar System (see, e.g., Wasserburg et al. [42] for a review), in particular for the estimation of its s- and r-process contributions [39,43].

Analogous results are obtained for the $M = 2\,M_\odot$ $Z = Z_\odot$ AGB model (see Figure 2). In this case, because of the decreased amount of iron seed in comparison to the number of neutrons produced by the ^{13}C burning, a higher production of heavy s-process elements (Ba-La-Ce-Nd-Sm) is obtained, thus magnifying the effects of the revised cross sections on isotopes belonging to the second s-process peak. Noteworthy variations ($\gtrsim$10%) are in fact found for ^{142}Nd. ^{142}Nd is a neutron-magic nucleus ($N = 82$), whose solar abundance is almost entirely due to its s-process component, since ^{142}Ce shields it against the r-process. During the s-process nucleosynthesis, the ^{142}Nd abundance is marginally affected by

branching in the neutron-capture path corresponding to ^{141}Ce and ^{142}Pr. Most of ^{142}Nd is synthesized during the radiative burning of the ^{13}C pocket when the s-path proceeds close to the neutron-magic nuclei. The new MACS is smaller than the previous estimation by [33] of ∼14% at thermal energies of 8 keV, typical of the ^{13}C radiative burning [44], while the value at 30 keV is almost the same. Actually, because of the presence of many resonances in the low-energy region for this isotope, the adoption of a specific evaluated cross section available in data libraries affects the computation of the MACS at low thermal energy. Therefore, the discrepancy between the two evaluations derives from the different library adopted (see Reifarth et al. [22], Wisshak et al. [45])
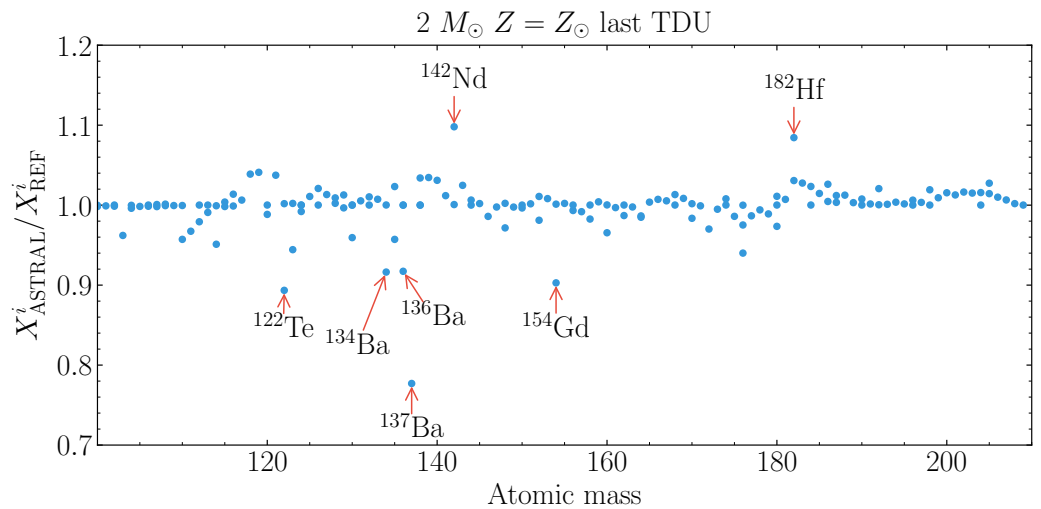
**Figure 2.** Same as Figure 1, but for a star with metallicity $Z = Z_{\odot}$.

    The above results are confirmed by the $M = 2\,M_{\odot}\ Z = 0.01$ NEW model (see Figure 3), for which the higher neutron-to-seed ratio and temperatures attained during TPs cause a significant difference also for the ^{176}Hf abundance. ^{176}Hf and its parent ^{176}Lu are two s-only isotopes. ^{176}Lu was originally considered as a possible nuclear chronometer for the age of s-elements because of its long half-life. However, at temperatures typical of the s-process, it exhibits a quite strong dependency on temperature [46] due to the coupling between the short-lived isomer ($t^{m}_{1/2}$ = 3.66 h) and the long-lived ground state ($t^{g}_{1/2}$ = 36 Gyr; see Söderlund et al. [47]). During the ^{13}C pocket phase the temperatures are so low (∼80–100 MK) that the two states actually behave as separate nuclei, being internal transitions highly forbidden by nuclear selection rules. On the other hand, at the higher temperatures of the TPs, overlying mediating states are excited and can decay to the long-lived ground state as well (see, e.g., Heil et al. [48]). This increases the ^{176}Lu^{g} production at the expense of ^{176}Hf, whose production is suppressed because of the enhanced (n, γ) branch feeding ^{176}Lu. The production of ^{176}Lu^{g} is then determined by the partial (n, γ) cross section of the ground state ^{176}Lu^{g} to the total cross section. In our models, this ratio is set to 0.20 for temperatures lower than 200 MK and 0.25 for higher temperatures (see Cristallo et al. [49]). The new ASTRAL v0 evaluations indicate that both the production and the destruction channels of the long-lived ^{176}Lu^{g} are greater than the REF case (see Table 1). Moreover, the destruction cross section of ^{176}Hf is slightly larger. As a whole, the NEW model shows an abundance of ^{176}Hf reduced by ∼10% compared to the REF model. On the other hand, the ^{176}Lu/^{176}Hf ratio increases by ∼5%.
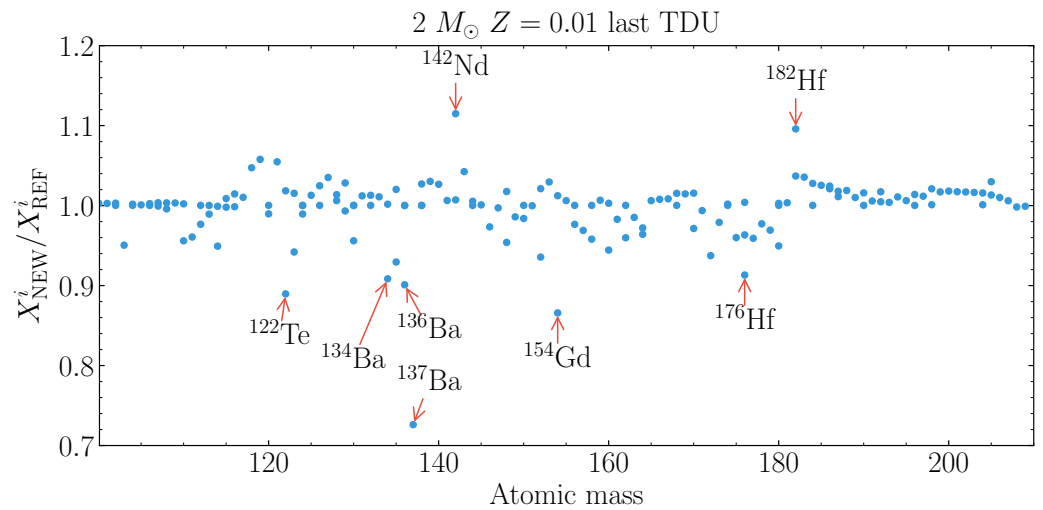
Figure 3. Same as Figure 1, but for a star with metallicity $Z = 0.01$.

Accordingly to the current paradigm, ancient carbon-rich AGB stars that evolved prior to the formation of the Solar System are the progenitor of about 90% of presolar SiC grains, termed the mainstream (MS) grains, recovered in pristine meteorites (see Zinner [50] for a review). Isotopic s-element abundance ratios measured in those grains have been shown to provide accurate constraints on the ^{13}C pocket (e.g., Liu et al. [51]). In addition, the typical Si isotope ratios of MS grains suggest that their parent stars should have close-to-solar (e.g., Hoppe et al. [52]) or slightly super-solar metallicity [53], while Lugaro et al. [54] proposed that the large MS SiC grains (μm-sized) might come from AGB stars of about twice solar metallicity. More recently, based on chemical and chemo-dynamical models of the Galaxy coupled with dust yields resulting from AGB models, Cristallo et al. [55] showed that the majority of presolar SiC grains originated from AGB stars with $M \sim 2 \, M_\odot$ and $Z \sim Z_\odot$ (see also Gail et al. [56]). In this regard, magnetic models for $2 \, M_\odot$ AGB stars with close-to-solar metallicities show ^{13}C profiles flat and extended enough to provide a good match to measured grain data [18]. In Figure 4, we compare NEW and REF models with available laboratory measurements of isotope ratios of barium in presolar SiC grains. The isotope ratios are reported in the standard δ-notation, defined as the deviation in parts per thousand of the isotopic ratio measured in a grain with respect to the terrestrial ratio. In the plot, grain data for $\delta(^{135}\text{Ba}/^{136}\text{Ba})$ versus $\delta(^{137}\text{Ba}/^{136}\text{Ba})$ values form a linear trendline with a similar slope to the stellar model predictions. Both REF and NEW models show a small offset with respect to the best-fit line of grain data, which lies in between the two theoretical predictions. In comparison with REF models, which present too little negative $\delta(^{137}\text{Ba}/^{136}\text{Ba})$ values, NEW models attain too much negative values. Adopting the re-evaluated value for the ^{137}Ba cross section recommended by ASTRAL v0, which is 47% higher at 8 keV than the REF value, decreases the ^{137}Ba abundance and so the $\delta(^{137}\text{Ba}/^{136}\text{Ba})$ model predictions up to 100‰. The majority of the presolar SiC grains have $\delta(^{138}\text{Ba}/^{136}\text{Ba})$ values below -250‰ that are well reproduced by REF models of solar or super-solar metallicity, while the $Z = 0.01$ model gives a good match only to the grains with the lowest $\delta(^{135}\text{Ba}/^{136}\text{Ba})$ and the highest $\delta(^{138}\text{Ba}/^{136}\text{Ba})$ values, indicating that this model has a neutron-to-seed ratio a little too high for describing the bulk of the data. In Vescovi et al. [18], the same model was shown to be able to explain the most anomalous Mo isotope ratios of Y and Z grains, which are thought to have originated in lower-than-solar metallicity AGB stars and have Mo isotopic compositions indistinguishable from MS grains (see Liu et al. [57] for more details). In this regard, however, recent analyses are revealing that the three groups of grains have also similar Sr and Ba isotopic compositions, thus questioning the low-metallicity stellar origin of Y and Z grains [58]. From the comparison with grain data, models computed with the REF data set seem to give a better match while models adopting the ASTRAL v0 set only provide a partial overlap. The latter, as a consequence of the reduced ^{136}Ba abundance,

results in a systematic increase of all model predictions for $\delta(^{138}\mathrm{Ba}/^{136}\mathrm{Ba})$ by $\sim 100‰$. Nonetheless, strong conclusions cannot be advanced due to the relative uncertainties in the neutron-capture MACS values for $^{136}\mathrm{Ba}$, $^{137}\mathrm{Ba}$, and $^{138}\mathrm{Ba}$. Even if they are typically less than 5%, the uncertainty in $\delta(^{137}\mathrm{Ba}/^{136}\mathrm{Ba})$ and $\delta(^{138}\mathrm{Ba}/^{136}\mathrm{Ba})$ predictions is up to a few tens of ‰. Uncertainties regarding neutron-capture reaction cross sections and beta decays for cesium isotopes further complicate the picture, possibly leading to larger spreads in $^{137}\mathrm{Ba}$ and $^{138}\mathrm{Ba}$ abundances [59]. Therefore, within experimental and model uncertainties, the majority of barium isotope ratios measured in presolar SiC grain are in agreement with both REF and NEW model predictions, the latter exhibiting larger differences in the data–model comparison.
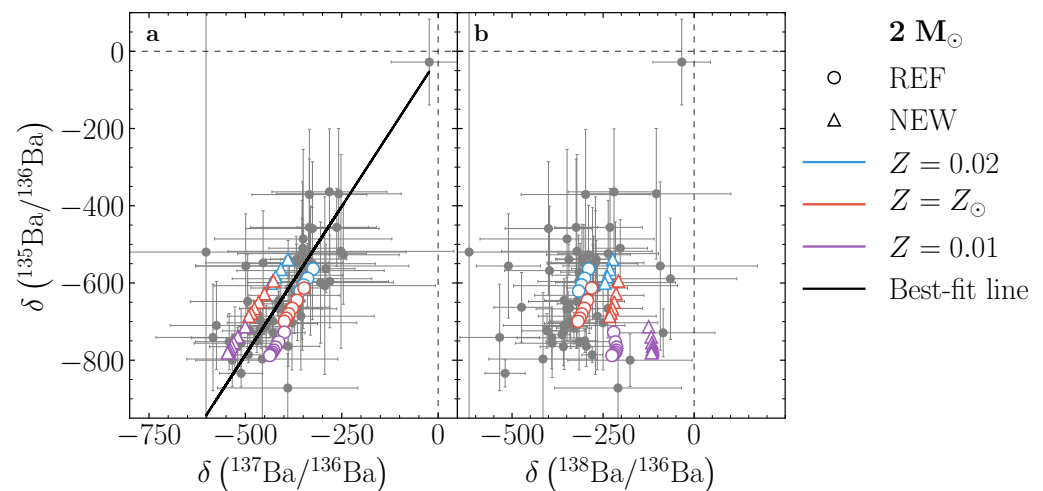
Figure 4. Three-isotope plot of $\delta^{135}\mathrm{Ba}/^{136}\mathrm{Ba}$ vs. $\delta^{137}\mathrm{Ba}/^{136}\mathrm{Ba}$ (**a**) and $\delta^{135}\mathrm{Ba}/^{136}\mathrm{Ba}$ vs. $\delta^{138}\mathrm{Ba}/^{136}\mathrm{Ba}$ (**b**). Theoretical stellar predictions calculated under different (n, γ) data set are compared to MS SiC grain data from [51,60,61]. In panel (**a**), the best-fit line of grain data (black solid) is shown (see text for details). Symbols corresponds to different TPs for the C-rich phase, i.e., when C/O > 1 in the envelope and condensation of SiC is most likely to occur. Plotted are 2σ errors.

4. Conclusions

In this work, we investigated the effects induced by the adoption of a new neutron-capture cross section database on the s-process nucleosynthesis in low-mass AGB stars. We found major variations (more than 10%) in the final surface abundance for a number of isotopes. Most of the differences are a consequence of the re-evaluated cross sections, which are systematically higher than previous evaluations due to the different adopted gold cross section as a reference. Remarkable exceptions are represented by (n, γ) cross section for $^{142}\mathrm{Nd}$ and $^{137}\mathrm{Ba}$, whose recent re-evaluation greatly differ from previous results especially at low energy. Because of the scarcity of experimental data in this energy region, the MACS calculation is strongly influenced by the (n, γ) cross sections in the evaluated data libraries adopted, which rely on various statistical model calculations to extrapolate the measured cross sections to higher and lower energies, potentially leading to different MACS values.

We compared the isotopic composition of barium measured in presolar SiC grains of AGB origins with the result of s-process nucleosynthesis occurring in the AGB phases of stars of 2 $M_\odot$ with close-to-solar metallicities. We found that, within the present uncertainties in the input neutron-capture cross sections, a good agreement between model predictions and observed isotopic ratios is obtained with both new and previous evaluated MACS data sets. In this regard, more experimental measurements at low energies are required to better constraint energy-dependent cross sections for Ba isotopes.

In the near future, we plan to extend the ASTRAL database performing a systematic re-evaluation of measurements performed with the activation technique and for which the

revision of the ^{197}Au(n, γ) cross section provides a new spectrum-averaged cross section to be used as normalization. The revised data set will likely have a deep effect on s-process nucleosynthesis both occurring in AGB and massive stars.

Author Contributions: Conceptualization, D.V. and R.R.; methodology, D.V.; software, D.V. and R.R.; validation, D.V. and R.R.; formal analysis, D.V.; investigation, D.V.; writing—original draft preparation, D.V.; writing—review and editing, D.V.; visualization, D.V. All authors have read and agreed to the published version of the manuscript.

Institutional Review Board Statement: Not applicable.

Informed Consent Statement: Not applicable.

Data Availability Statement: Presolar grain data are from the Presolar Grain Database of the Laboratory for Space at Washington University in St. Louis, USA (https://presolar.physics.wustl.edu/presolar-grain-database).

Conflicts of Interest: The authors declare no conflict of interest.

References

1. Busso, M.; Gallino, R.; Wasserburg, G.J. Nucleosynthesis in Asymptotic Giant Branch Stars: Relevance for Galactic Enrichment and Solar System Formation. *Annu. Rev. Astron. Astrophys.* **1999**, *37*, 239–309. [CrossRef]
2. Straniero, O.; Gallino, R.; Busso, M.; Chiefei, A.; Raiteri, C.M.; Limongi, M.; Salaris, M. Radiative 13C Burning in Asymptotic Giant Branch Stars and s-Processing. *Astrophys. J. Lett.* **1995**, *440*, L85. [CrossRef]
3. Cristallo, S.; La Cognata, M.; Massimi, C.; Best, A.; Palmerini, S.; Straniero, O.; Trippella, O.; Busso, M.; Ciani, G.F.; Mingrone, F.; et al. The Importance of the ^{13}C(α,n)^{16}O Reaction in Asymptotic Giant Branch Stars. *Astrophys. J.* **2018**, *859*, 105. [CrossRef]
4. Herwig, F.; Bloecker, T.; Schoenberner, D.; El Eid, M. Stellar evolution of low and intermediate-mass stars. IV. Hydrodynamically-based overshoot and nucleosynthesis in AGB stars. *Astron. Astrophys.* **1997**, *324*, L81–L84.
5. Herwig, F.; Langer, N.; Lugaro, M. The s-Process in Rotating Asymptotic Giant Branch Stars. *Astrophys. J.* **2003**, *593*, 1056–1073. [CrossRef]
6. Siess, L.; Goriely, S.; Langer, N. Nucleosynthesis of s-elements in rotating AGB stars. *Astron. Astrophys.* **2004**, *415*, 1089–1097. [CrossRef]
7. Piersanti, L.; Cristallo, S.; Straniero, O. The Effects of Rotation on s-process Nucleosynthesis in Asymptotic Giant Branch Stars. *Astrophys. J.* **2013**, *774*, 98. [CrossRef]
8. Cristallo, S.; Straniero, O.; Gallino, R.; Piersanti, L.; Domínguez, I.; Lederer, M.T. Evolution, Nucleosynthesis, and Yields of Low-Mass Asymptotic Giant Branch Stars at Different Metallicities. *Astrophys. J.* **2009**, *696*, 797–820. [CrossRef]
9. Cristallo, S.; Piersanti, L.; Straniero, O.; Gallino, R.; Domínguez, I.; Abia, C.; Di Rico, G.; Quintini, M.; Bisterzo, S. Evolution, Nucleosynthesis, and Yields of Low-mass Asymptotic Giant Branch Stars at Different Metallicities. II. The FRUITY Database. *Astrophys. J. Suppl. Ser.* **2011**, *197*, 17. [CrossRef]
10. Cristallo, S.; Straniero, O.; Piersanti, L.; Gobrecht, D. Evolution, Nucleosynthesis, and Yields of AGB Stars at Different Metallicities. III. Intermediate-mass Models, Revised Low-mass Models, and the ph-FRUITY Interface. *Astrophys. J. Suppl. Ser.* **2015**, *219*, 40. [CrossRef]
11. Denissenkov, P.A.; Tout, C.A. Partial mixing and formation of the ^{13}C pocket by internal gravity waves in asymptotic giant branch stars. *Mon. Not. RAS* **2003**, *340*, 722–732. [CrossRef]
12. Battino, U.; Pignatari, M.; Ritter, C.; Herwig, F.; Denisenkov, P.; Den Hartogh, J.W.; Trappitsch, R.; Hirschi, R.; Freytag, B.; Thielemann, F.; et al. Application of a Theory and Simulation-based Convective Boundary Mixing Model for AGB Star Evolution and Nucleosynthesis. *Astrophys. J.* **2016**, *827*, 30. [CrossRef]
13. Battino, U.; Tattersall, A.; Lederer-Woods, C.; Herwig, F.; Denissenkov, P.; Hirschi, R.; Trappitsch, R.; den Hartogh, J.W.; Pignatari, M.; NuGrid Collaboration. NuGrid stellar data set—III. Updated low-mass AGB models and s-process nucleosynthesis with metallicities Z = 0.01, Z = 0.02, and Z = 0.03. *Mon. Not. RAS* **2019**, *489*, 1082–1098. [CrossRef]
14. Trippella, O.; Busso, M.; Maiorca, E.; Käppeler, F.; Palmerini, S. s-Processing in AGB Stars Revisited. I. Does the Main Component Constrain the Neutron Source in the ^{13}C Pocket? *Astrophys. J.* **2014**, *787*, 41. [CrossRef]
15. Trippella, O.; Busso, M.; Palmerini, S.; Maiorca, E.; Nucci, M.C. s-Processing in AGB Stars Revisited. II. Enhanced 13C Production through MHD-induced Mixing. *Astrophys. J.* **2016**, *818*, 125. [CrossRef]
16. Palmerini, S.; Trippella, O.; Busso, M.; Vescovi, D.; Petrelli, M.; Zucchini, A.; Frondini, F. s-Processing from MHD-induced mixing and isotopic abundances in presolar SiC grains. *Geochim. Cosmochim. Acta* **2018**, *221*, 21–36. [CrossRef]
17. Busso, M.; Vescovi, D.; Palmerini, S.; Cristallo, S.; Antonuccio Delogu, V. s-Processing in AGB Stars Revisited. III. Neutron captures from MHD mixing at different metallicities and observational constraints. *arXiv* **2020**, arXiv:2011.07469.

18. Vescovi, D.; Cristallo, S.; Busso, M.; Liu, N. Magnetic-buoyancy-induced Mixing in AGB Stars: Presolar SiC Grains. *Astrophys. J. Lett.* **2020**, *897*, L25. [CrossRef]

19. Vescovi, D.; Cristallo, S.; Palmerini, S.; Abia, C.; Busso, M. Magnetic-buoyancy-induced mixing in AGB Stars: Fluorine nucleosynthesis at different metallicities. *arXiv* **2021**, arXiv:2106.08241.

20. Magrini, L.; Vescovi, D.; Casali, G.; Cristallo, S.; Vazquez, C.V.; Cescutti, G.; Spina, L.; Der Swaelmen, M.V. Magnetic-buoyancy-induced mixing in AGB Stars: A theoretical explanation of the non-universal [Y/Mg]-age relation. *arXiv* **2021**, arXiv:2101.04429.

21. Käppeler, F.; Gallino, R.; Bisterzo, S.; Aoki, W. The s process: Nuclear physics, stellar models, and observations. *Rev. Mod. Phys.* **2011**, *83*, 157–194. [CrossRef]

22. Reifarth, R.; Erbacher, P.; Fiebiger, S.; Göbel, K.; Heftrich, T.; Heil, M.; Käppeler, F.; Klapper, N.; Kurtulgil, D.; Langer, C.; et al. Neutron-induced cross sections. From raw data to astrophysical rates. *Eur. Phys. J. Plus* **2018**, *133*, 424. [CrossRef]

23. Lederer, C.; Colonna, N.; Domingo-Pardo, C.; Gunsing, F.; Käppeler, F.; Massimi, C.; Mengoni, A.; Wallner, A.; Abbondanno, U.; Aerts, G.; et al. Au197(n,γ) cross section in the unresolved resonance region. *Phys. Rev. C* **2011**, *83*, 034608. [CrossRef]

24. Massimi, C.; Becker, B.; Dupont, E.; Kopecky, S.; Lampoudis, C.; Massarczyk, R.; Moxon, M.; Pronyaev, V.; Schillebeeckx, P.; Sirakov, I.; et al. Neutron capture cross section measurements for ^{197}Au from 3.5 to 84 keV at GELINA. *Eur. Phys. J. A* **2014**, *50*, 124. [CrossRef]

25. Ratynski, W.; Käppeler, F. Neutron capture cross section of ^{197}Au: A standard for stellar nucleosynthesis. *Phys. Rev. C* **1988**, *37*, 595–604. [CrossRef] [PubMed]

26. Straniero, O.; Gallino, R.; Cristallo, S. s process in low-mass asymptotic giant branch stars. *Nucl. Phys. A* **2006**, *777*, 311–339. [CrossRef]

27. Marigo, P.; Aringer, B. Low-temperature gas opacity. ÆSOPUS: A versatile and quick computational tool. *Astron. Astrophys.* **2009**, *508*, 1539–1569. [CrossRef]

28. Cristallo, S.; Straniero, O.; Lederer, M.T.; Aringer, B. Molecular Opacities for Low-Mass Metal-poor AGB Stars Undergoing the Third Dredge-up. *Astrophys. J.* **2007**, *667*, 489–496. [CrossRef]

29. Lodders, K. Solar Elemental Abundances. *Oxf. Res. Encycl. Planet. Sci.* **2020**. [CrossRef]

30. Vescovi, D.; Piersanti, L.; Cristallo, S.; Busso, M.; Vissani, F.; Palmerini, S.; Simonucci, S.; Taioli, S. Effects of a revised ^{7}Be e^{-}-capture rate on solar neutrino fluxes. *Astron. Astrophys.* **2019**, *623*, A126. [CrossRef]

31. Abia, C.; de Laverny, P.; Cristallo, S.; Kordopatis, G.; Straniero, O. Properties of carbon stars in the solar neighbourhood based on Gaia DR2 astrometry. *Astron. Astrophys.* **2020**, *633*, A135. [CrossRef]

32. Nucci, M.C.; Busso, M. Magnetohydrodynamics and Deep Mixing in Evolved Stars. I. Two- and Three-dimensional Analytical Models for the Asymptotic Giant Branch. *Astrophys. J.* **2014**, *787*, 141. [CrossRef]

33. Bao, Z.Y.; Beer, H.; Käppeler, F.; Voss, F.; Wisshak, K.; Rauscher, T. Neutron Cross Sections for Nucleosynthesis Studies. *At. Data Nucl. Data Tables* **2000**, *76*, 70–154. [CrossRef]

34. Mazzone, A.; Cristallo, S.; Aberle, O.; Alaerts, G.; Alcayne, V.; Amaducci, S.; Andrzejewski, J.; Audouin, L.; Babiano-Suarez, V.; Bacak, M.; et al. Measurement of the ^{154}Gd(n,γ) cross section and its astrophysical implications. *Phys. Lett. B* **2020**, *804*, 135405. [CrossRef]

35. Roig, O.; Jandel, M.; Méot, V.; Bond, E.M.; Bredeweg, T.A.; Couture, A.J.; Haight, R.C.; Keksis, A.L.; Rundberg, R.S.; Ullmann, J.L.; et al. Radiative neutron capture cross sections on ^{176}Lu at DANCE. *Phys. Rev. C* **2016**, *93*, 034602. [CrossRef]

36. Wisshak, K.; Voss, F.; Käppeler, F.; Kazakov, L.; Bečvář, F.; Krtička, M.; Gallino, R.; Pignatari, M. Fast neutron capture on the Hf isotopes: Cross sections, isomer production, and stellar aspects. *Phys. Rev. C* **2006**, *73*, 045807. [CrossRef]

37. Takahashi, K.; Yokoi, K. Beta-Decay Rates of Highly Ionized Heavy Atoms in Stellar Interiors. *At. Data Nucl. Data Tables* **1987**, *36*, 375. [CrossRef]

38. Bisterzo, S.; Gallino, R.; Käppeler, F.; Wiescher, M.; Imbriani, G.; Straniero, O.; Cristallo, S.; Görres, J.; deBoer, R.J. The branchings of the main s-process: Their sensitivity to α-induced reactions on ^{13}C and ^{22}Ne and to the uncertainties of the nuclear network. *Mon. Not. RAS* **2015**, *449*, 506–527. [CrossRef]

39. Vescovi, D.; Busso, M.; Palmerini, S.; Trippella, O.; Cristallo, S.; Piersanti, L.; Chieffi, A.; Limongi, M.; Hoppe, P.; Kratz, K.L. On the Origin of Early Solar System Radioactivities: Problems with the Asymptotic Giant Branch and Massive Star Scenarios. *Astrophys. J.* **2018**, *863*, 115. [CrossRef]

40. Lugaro, M.; Heger, A.; Osrin, D.; Goriely, S.; Zuber, K.; Karakas, A.I.; Gibson, B.K.; Doherty, C.L.; Lattanzio, J.C.; Ott, U. Stellar origin of the ^{182}Hf cosmochronometer and the presolar history of solar system matter. *Science* **2014**, *345*, 650–653. [CrossRef]

41. Bondarenko, V.; Berzins, J.; Prokofjevs, P.; Simonova, L.; von Egidy, T.; Honzátko, J.; Tomandl, I.; Alexa, P.; Wirth, H.F.; Köster, U.; et al. Interplay of quasiparticle and phonon excitations in ^{181}Hf observed through (n,γ) and (d$\to$,p) reactions. *Nucl. Phys. A* **2002**, *709*, 3–59. [CrossRef]

42. Wasserburg, G.J.; Busso, M.; Gallino, R.; Nollett, K.M. Short-lived nuclei in the early Solar System: Possible AGB sources. *Nucl. Phys. A* **2006**, *777*, 5–69. [CrossRef]

43. Côté, B.; Lugaro, M.; Reifarth, R.; Pignatari, M.; Világos, B.; Yagüe, A.; Gibson, B.K. Galactic Chemical Evolution of Radioactive Isotopes. *Astrophys. J.* **2019**, *878*, 156. [CrossRef]

44. Gallino, R.; Arlandini, C.; Busso, M.; Lugaro, M.; Travaglio, C.; Straniero, O.; Chieffi, A.; Limongi, M. Evolution and Nucleosynthesis in Low-Mass Asymptotic Giant Branch Stars. II. Neutron Capture and the S-Process. *Astrophys. J.* **1998**, *497*, 388–403. [CrossRef]

45. Wisshak, K.; Voss, F.; Käppeler, F. Neutron capture resonances in ^{142}Nd and ^{144}Nd. *Phys. Rev. C* **1998**, *57*, 3452–3458. [CrossRef]

46. Klay, N.; Käppeler, F.; Beer, H.; Schatz, G. Nuclear structure of ^{176}Lu and its astrophysical consequences. II. ^{176}Lu, a thermometer for stellar helium burning. *Phys. Rev. C* **1991**, *44*, 2839–2849. [CrossRef]

47. Söderlund, U.; Patchett, P.J.; Vervoort, J.D.; Isachsen, C.E. The ^{176}Lu decay constant determined by Lu-Hf and U-Pb isotope systematics of Precambrian mafic intrusions. *Earth Planet. Sci. Lett.* **2004**, *219*, 311–324. [CrossRef]

48. Heil, M.; Winckler, N.; Dababneh, S.; Käppeler, F.; Wisshak, K.; Bisterzo, S.; Gallino, R.; Davis, A.M.; Rauscher, T. ^{176}Lu/^{176}Hf: A Sensitive Test of s-Process Temperature and Neutron Density in AGB Stars. *Astrophys. J.* **2008**, *673*, 434–444. [CrossRef]

49. Cristallo, S.; Piersanti, L.; Gallino, R.; Straniero, O.; Käppeler, F.; Domínguez, I.; Mohr, P. The long-standing problem of ^{176}Lu/^{176}Hf branching: A new approach with full stellar evolutionary models. *J. Phys. Conf. Ser.* **2010**, *202*, 012033. [CrossRef]

50. Zinner, E. 1.4—Presolar Grains. In *Treatise on Geochemistry*, 2nd ed.; Holland, H.D., Turekian, K.K., Eds.; Elsevier: Oxford, UK, 2014; pp. 181–213. [CrossRef]

51. Liu, N.; Savina, M.R.; Gallino, R.; Davis, A.M.; Bisterzo, S.; Gyngard, F.; Käppeler, F.; Cristallo, S.; Dauphas, N.; Pellin, M.J.; et al. Correlated Strontium and Barium Isotopic Compositions of Acid-cleaned Single Mainstream Silicon Carbides from Murchison. *Astrophys. J.* **2015**, *803*, 12. [CrossRef]

52. Hoppe, P.; Annen, P.; Strebel, R.; Eberhardt, P.; Gallino, R.; Lugaro, M.; Amari, S.; Lewis, R.S. Meteoritic Silicon Carbide Grains with Unusual Si Isotopic Compositions: Evidence for an Origin in Low-Mass, Low-Metallicity Asymptotic Giant Branch Stars. *Astrophys. J. Lett.* **1997**, *487*, L101–L104. [CrossRef]

53. Lewis, K.M.; Lugaro, M.; Gibson, B.K.; Pilkington, K. Decoding the Message from Meteoritic Stardust Silicon Carbide Grains. *Astrophys. J. Lett.* **2013**, *768*, L19. [CrossRef]

54. Lugaro, M.; Cseh, B.; Világos, B.; Karakas, A.I.; Ventura, P.; Dell'Agli, F.; Trappitsch, R.; Hampel, M.; D'Orazi, V.; Pereira, C.B.; et al. Origin of Large Meteoritic SiC Stardust Grains in Metal-rich AGB Stars. *Astrophys. J.* **2020**, *898*, 96. [CrossRef]

55. Cristallo, S.; Nanni, A.; Cescutti, G.; Minchev, I.; Liu, N.; Vescovi, D.; Gobrecht, D.; Piersanti, L. Mass and metallicity distribution of parent AGB stars of presolar SiC. *Astron. Astrophys.* **2020**, *644*, A8. [CrossRef]

56. Gail, H.P.; Zhukovska, S.V.; Hoppe, P.; Trieloff, M. Stardust from Asymptotic Giant Branch Stars. *Astrophys. J.* **2009**, *698*, 1136–1154. [CrossRef]

57. Liu, N.; Stephan, T.; Cristallo, S.; Gallino, R.; Boehnke, P.; Nittler, L.R.; O'Alexander, C.M.D.; Davis, A.M.; Trappitsch, R.; Pellin, M.J.; et al. Presolar Silicon Carbide Grains of Types Y and Z: Their Molybdenum Isotopic Compositions and Stellar Origins. *Astrophys. J.* **2019**, *881*, 28. [CrossRef]

58. Liu, N.; Stephan, T.; Cristallo, S.; Gallino, R.; Boehnke, P.; Nittler, L.R.; Alexander, C.M.O.; Davis, A.M.; Trappitsch, R.; Pellin, M.J. Presolar Silicon Carbide Grains of Groups Y and Z: Their Strontium and Barium Isotopic Compositions and Stellar Origins. In Proceedings of the Lunar and Planetary Science Conference, The Woodlands, TX, USA, 18–22 March 2019; p. 1349.

59. Palmerini, S.; Busso, M.; Vescovi, D.; Naselli, E.; Pidatella, A.; Mucciola, R.; Cristallo, S.; Mascali, D.; Mengoni, A.; Simonucci, S.; et al. 2021. Submitted to *Astrophys. J.*

60. Liu, N.; Savina, M.R.; Davis, A.M.; Gallino, R.; Straniero, O.; Gyngard, F.; Pellin, M.J.; Willingham, D.G.; Dauphas, N.; Pignatari, M.; et al. Barium Isotopic Composition of Mainstream Silicon Carbides from Murchison: Constraints for s-process Nucleosynthesis in Asymptotic Giant Branch Stars. *Astrophys. J.* **2014**, *786*, 66. [CrossRef]

61. Stephan, T.; Trappitsch, R.; Davis, A.M.; Pellin, M.J.; Rost, D.; Savina, M.R.; Dauphas, N. Strontium and barium isotopes in presolar silicon carbide grains measured with CHILI—Two types of X grains. *Geochim. Cosmochim. Acta* **2018**, 109–126. [CrossRef]